JOURNAL OF MECHANICAL ENGINEERING, SCIENCE, AND INNOVATION
ITATS
Research Article

Vibration Analysis for Turning-Milling Process Condition Monitoring using Short-Time Fourier Transform Enhanced by Empirical Mode Decomposition

Journal of Mechanical Engineering, Science, and Innovation
e-ISNN: 2776-3536
2023, Vol. 3, No. 2
DOI: 10.31284/j.jmesi.2023.v3i2.5112
ejurnal.itats.ac.id/jmesi

Agus Susanto[1], Muizuddin Azka[2], Farid Majedi[1], Nur Kholis Faizin[1], Hanum Arrosida[1], Reza Putri Andriyani[1]

[1]Faculty of Engineering, State Polytechnic of Madiun, Indonesia
[2]Research Center of Process and Manufacturing Industry Technology, National Research and Innovation Agency, Indonesia

Corresponding author:
Agus Susanto
Faculty of Engineering, State Polytechnic of Madiun, Indonesia
Email: agus_eng.dept@pnm.ac.id

Abstract

Turn-milling process is widely applied in industries that provides advantages for machining large-diameter mechanical parts with high speed, reducing cutting temperature, which in turn decreases tool wear. However, it needs to monitor the turn-milling process for preventing the onset of chatter vibration during operation and the chatter induces negative effects. Vibration analysis is one of the ways for monitoring it. However, acquired vibrations should be denoised from noises, where in the conventional signal filter may have defiance to do that. This paper presents the utilization of the empirical mode decomposition (EMD) method as an efficient and adaptive noise filter. The Short-Time Fourier Transform (STFT) improvement using EMD is then used for monitoring turn-milling process conditions in the energy-time-frequency domain. The results showed that the reconstructed signal showed more superiority compared to the raw signal and the oscillation of the filtered signal was clearer than the raw signal. The improvement of the filtered signals was proved by the kurtosis index and spectral kurtosis. The improved STFT using EMD showed a significant spectrum with high resolution compared to conventional STFT. The energy density could be observed clearly in the machining characteristic frequencies with an improvement of about 10-100 times larger. The proposed method is therefore effectively applied to monitor the turn-milling condition.

Keywords: *Turn-Milling process Monitoring, Denoising signal, EMD, IMFs, Reconstructed Signal*

Received: September 24, 2023; Received in revised: October 31, 2023; Accepted: October 31, 2023
Handling Editor: Rizal Mahmud

INTRODUCTION

Turn-milling is one of the effective manufacturing operations which is combining process of the turning and milling. In the turn-milling process, a cylindrical workpiece that generally rotates in its axes is cut by the rotating cutting tool which rotates in its axes too. This cutting process takes place simultaneously and therefore would improve productivity during machining compared to the turning or milling process itself. It is because the high speed can be achieved in the turn-milling process due to both the cutting tool and workpiece rotating simultaneously, even though cuts the mechanical parts with large diameters.

The other advantages are the interrupted cutting in turn-milling which makes the chips broken during machining. Cutting temperature, therefore, reduces which in turn decreases tool wear [1]. Due to these special aspects and several advantages offer by turn-milling, it is widely used in industries with large-sized workpieces [2].

Because of its utilization for mass production in many industries, several researchers have studied the effect of machining parameter on the surface quality and tool life during turn-milling process. Ratnam *et al*. [3]. conducted the first investigation in turn-milling. They studied about chip removal, surface quality, and cutting forces during high-speed turn-milling process. Choudhury and Mangrulkar [4] investigated the surface roughness quality of resulted product in turn-milling and compared the results with conventional turning. Their work showed that surface roughness obtained by turn-milling is lower than that is obtained by conventional turning. Besides, Choudhury *et al*. [5] compared the surface quality obtained in turn-milling to conventional milling experimentally and showed that the surface quality produced in turn-milling was better. The effect of eccentricity on the surface roughness in turn-milling was investigated by Kopac and Pogacnik [6] and they showed that that surface quality was much better obtained by eccentric turn-milling process. In order to predict the surface roughness during turn-milling process, Yuan and Zheng [7] developed a geometric model and confirmed it experimentally. In addition, Huang *et al.* [8] studied the effects of machining parameters on the tool wear during turn-milling process. Karaguzel *et al.* [9] carried out number of turn-milling tests for machining nickel alloys with zero eccentricity. They showed that the tool life significant increases up to 20 times using turn-milling compared to normal turning process. Their results were agreed by Neagu *et al.* [10] that pointed out that turn-milling could reach 20 times greater productivity than conventional turning process of straight shafts. Filho [11] modelled the cutting forces for turn-milling, then confirmed them experimentally.

Despite all advantages that turn-milling offers, turn-milling process monitoring is essential for preventing from development self-excited vibration known as chatter vibration, which can arise during machining at any time [12],[13]. The chatter becomes a common limitation to productivity and part quality, accelerates tool wear, and damages the machine-tools shaft [14], [15]. One of the excellent ways for monitoring many mechanical systems, including machining process is by vibration analysis. Ismail *et al.* [16] showed the effectiveness of vibration signal analysis for condition monitoring of the surface roughness in the deep grinding of stainless steel. Gupta *et al.* [17] developed the robust technique for motor fault diagnosis using signal processing. They used spectral analyses using fast Fourier transform (FFT) and STFT technique for analyzing signals. On the other hand, the utilization of signal processing for machining process monitoring was performed by Susanto, *et al*. [18]. In their work, the machining conditions under dried cutting, wet cutting, and under obstacles were also be evaluated as well. The difficulty encountered when analyzing various signal data, including analyzing vibrations, is the presence of noises. Signal processing tools that analyze data signals in the time-frequency domain may also experience difficulties when they are applied to the contaminated signal

by noises. Short-Time Fourier Transform (STFT) was applied for chatter mitigation during the milling of a thin-walled workpiece by submerging the machining system using viscous fluid [19]. Harun *et al.* [20] evaluated the early conditions of tool failure by analyzing tri-axial vibrations through time-frequency domains using STFT in the deep drilling process. Even though they can identify the chatter and cutting tool wear, however, their STFT spectrum seems messy due to being backgrounded by some noise. In addition, the STFT provides advantages for machining condition monitoring under the time and frequency domains, namely simple, quick, and sufficient.

The recent signal processing method is Hilbert–Huang transform (HHT), which works in two stages; empirical mode decomposition (EMD) and Hilbert transform [21]. Through applying the EMD to vibration data, then the data is decomposed into a set of intrinsic mode functions (IMFs). A distributed energy-time-frequency in a plane is then generated by applying the Hilbert transform to all IMFs components, which is called the Hilbert–Huang spectrum. HHT is widely applied for machining process monitoring. Susanto *et al.* [18], [22], [23] monitored the milling process condition of flexible workpieces by vibration analysis using HHT. In their study, the HHT was utilized for extracting many features that were beneficial for detecting chatter, and end-milling cutter damages. However, HHT is still having a drawback to face the noise which disturbs the practical vibrations, especially when the raw data contains low signal-to-noise ratio (SNR). Besides, the HHT is time-consuming in its computation. It is because the HHT performs the instantaneous frequency for generating the HHT spectrum with uniform resolution in entire frequency [18], [24].

Noises are often a problem in analysis and they are difficult to be eliminated effectively with conventional filter tools [24]. Therefore, the adaptive and effective signal processing tool for denoising noisy vibration signals is essential before further analysis signal. This paper presents the combination of EMD and STFT for turn-milling process monitoring. The EMD is utilized as a filter of noise which distorts the main data adaptively. The IMFs, which are obtained by EMD, separate the noisy signal components from the clear signal components. And then, the clear IMF components can be reconstructed to get a new signal. This way was rarely applied for the noisy signal obtained in the machining process and was applied by Huang *et al*. [25] for denoising the annual global surface temperatures. Furthermore, the STFT with its efficient computation is used for monitoring the machining process in energy-time-frequency spectrum.

METHODS AND ANALYSIS

Empirical Mode Decomposition (EMD)

The EMD is original idea of the HHT, which is used for decomposing raw data into a set of IMFs. The IMFs are series of components containing many different oscillations. Following are nine steps to conducting EMD [18], [25]:

Step 1 : A simple artificial signal of $y = \sin(2\pi t)$ is considered as time-series data that is to be decomposed by EMD. This data is shown in Figure 1.

Step 2 : The algorithm of EMD then ensures that the data is not a type of monotonic function. The monotonic function data means the data containing not more than one cycle oscillation. No one IMF can be resulted from monotonic function data. In this case, the process is running to the next step due to the data in Figure 1 being the type of non-monotonic signal.

Step 3 : The data is then determined by its local extrema and local minima.

Step 4 : Creating the upper envelope u(t) and lower envelope l(t). These envelopes can be plotted by connecting all local maxima and local minima using spline lines.

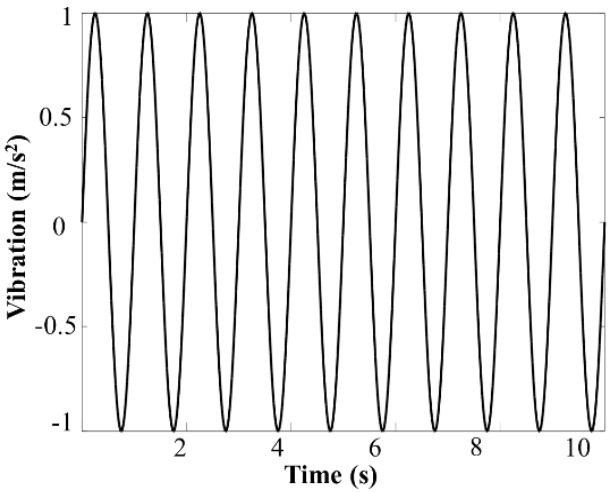

Figure 1. Considered time-series data to be decomposed by EMD

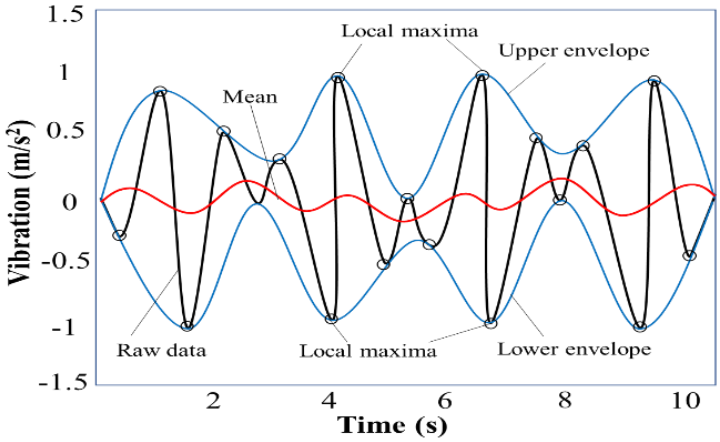

Figure 2. Illustration of steps 3-5; determining local ponts, generating envelopes, and calculating the mean of envelopes

Step 5 : Calculating the mean of envelopes. It is reached by m(t) = [u(t) + l(t)]/2.
Step 3-5 is illustrated in Figure 2.
Step 6 : Obtaining the proto-IMF. It is reached by $h(t) = x(t) - m(t)$
Step 7 : Obtaining an IMF $c_j(t)$. To get a $c_j(t)$, the *h(t)* should be sifted through the following process; where the indices indicate the iteration of the same step. The sifting process would result the first IMF $c_1(t)$ in the last iteration. The illustration of this sifting process is shown in Figure 3.

$$\left.\begin{aligned} & x(t) - m_{1,1}(t) = h_{1,1}(t); \\ & h_{1,1}(t) - m_{1,2}(t) = h_{1,2}(t); \\ & h_{1,2}(t) - m_{1,3}(t) = h_{1,3}(t); \\ & \ldots \\ & h_{1,k-1}(t) - m_{1,k}(t) = h_{1,k}(t); \\ & \Rightarrow h_{1,k}(t) = c_1(t) \end{aligned}\right\} \quad (1)$$

where the *k* is the integer number with represent the mode of the treated signal.

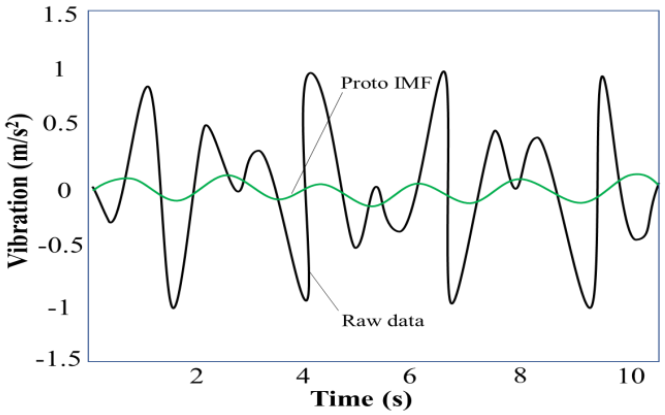

Figure 3. Illustration of sifting process which shows raw data and proto-IMF

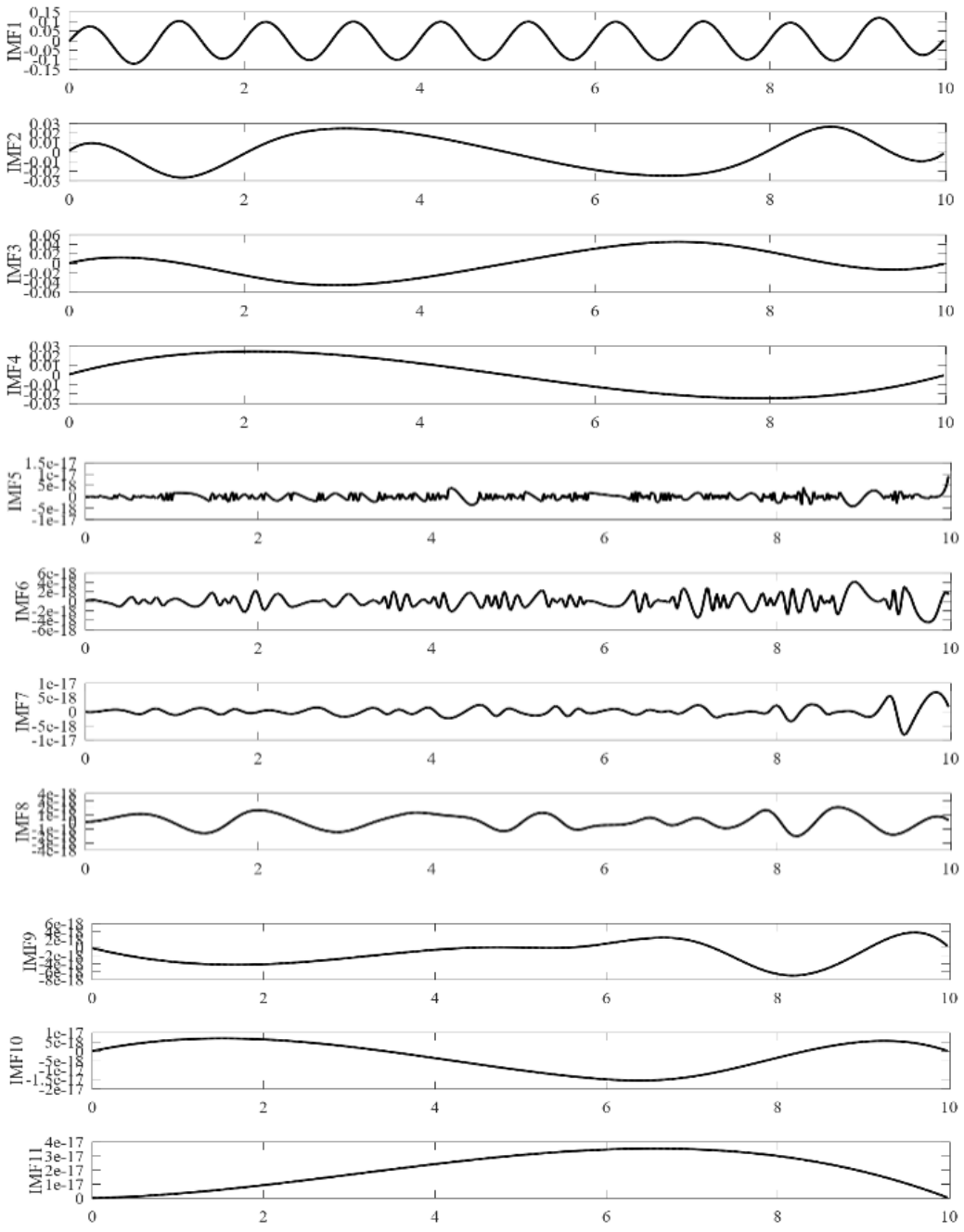

Figure 4. Signals which show raw signal, IMFs (c_1 – c_4), monotonic residue (r_{nk})

Step 8 : Next step is determining the residue by subtracting the raw data to the first IMF, $r_1(t) = x(t) - c_1(t)$. Data $r_1(t)$ is then treated as new data in the following step.

Step 9 : The second IMF $c_2(t)$ can be achieved by treating the data $r_1(t)$ as the following data, and repeating steps 2–7. $r_2(t)$ is then achieved.

Step 10 : All steps are repeated n_k times, so that a set of IMFs and a monotonic function, r_{nk}, are obtained.

The IMFs $\left(c_j(t)\right)$ and a monotonic residue (r_{nk}) obtained by EMD can be formed mathematically as in following Equation.

$$x(t) = \sum_{j=1}^{Nk} c_j(t) + r_{nk}(t) \qquad (2)$$

The IMFs of the artificial signal of *y(t)* are shown in Figure 4. As can be seen, the IMFs are an array of vibrations in certain frequency bands which are arranged from high to low frequency and we can identify the main IMF from others based on its frequency. Smooth IMF with high energy can be separated from messy IMF with low energy.

Experimental Work

This study is carried out in five steps. First, the vibration data which are acquired from turn-milling process are first examining by kurtosis index and spectral kurtosis for initial noise investigation. Second, the noisy vibration data is then decomposed by the EMD to get a set of IMFs. Third, smooth and clear IMFs are selected, then reconstruct them to get a new signal. The reconstructed signal is then compared to the raw signal to ensure that it is comparable to raw vibration. Fourth, the kurtosis index and spectral kurtosis is applied again to the reconstructed signal for noise inspection. The reconstructed signals are then evaluated in using STFT for analyzing the vibration in the energy-time–frequency distribution in the last step.

The vibration data were obtained in the experimental cutting test using CNC turn-milling machine of 5 Axis Mori Seiki NT 4300. The measuring vibration data during the cutting test is shown in Figure 5, in which Figure 5(a) shows the experimental setup in the machine, and Figure 5(b) shows the schematic diagram of the cutting test. The workpiece material was clamped on the three-jaw chuck of lathe headstock with no

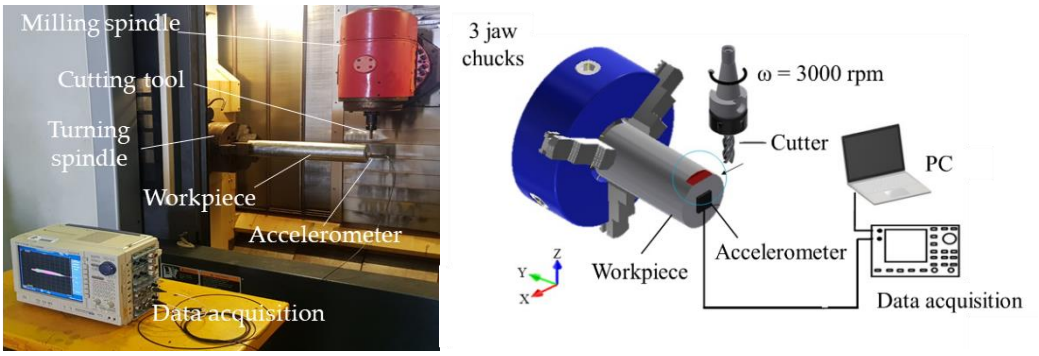

(a) (b)

Figure 5. Measuring vibration data during cutting test; (a) Experimental setup in CNC Turn-Milling machine of 5 Axis Mori Seiki NT 4300, (b) Schematic diagram of cutting test

rotation. This workpiece was machined by a rotated end-mill cutter with 3000 rpm for spindle rotation (ω) and 2 mm for the raster. The end-mill material was carbide which has four teeth and is 16 mm in diameter. Based on the figure, the vibration responses during machining were measured by an accelerometer mounted on the free end of the workpiece. The typically sensor was three axial accelerometer made by Dytran instrument, INC, 3413A2 for model, and 51.43 mV/g for the sensitivity. This vibration was then acquired using data acquisition, Yokogawa oscilloscope, with 100 kHz of the sampling frequency and can be transmitted to the personal computer (PC). During experimental tests, dry machining was applied.

RESULTS AND DISCUSSIONS

Figure 6 shows the raw data of the full vibration data obtained in the machining process under cutting parameters given in the experimental conditions. This signal represents the vibration in the x-axis. It is seen that the signal fluctuates during machining. It is not a typically signal obtained from either turning or milling. It could be compared to typically vibration obtained in milling [22] and in turning [23]. The fluctuated signals were caused by the cutting tool cuts varied cutting depth of the workpiece, in which the chip morphology of turn-milling was different from either a chip morphology of turning or a chip morphology of milling. Figure 7 presents the potential different of the chip morphology obtained in turning, milling, and turn-milling.

From the vibration, it is shown that there are three varied amplitudes of signal; the stable-unstable-stable amplitude of vibration signal in one tooth pass of the cutting tool. As can be seen from the signal, the cutting tool cuts the workpiece material at a cutting period of 0–0.25 seconds with stable machining. However, the cutting tool cuts other zones of workpiece material in the middle of the operation, which causes the amplitude of the signals to grow up suddenly at a cutting period of 0.3–1.7 seconds. This zone is corresponding to an unstable area. The increase of signal amplitudes can be addressed to the cutting force specific that also increases during cutting. The signal is then gradually decreased when the cutting tool cuts the last area of the workpiece.

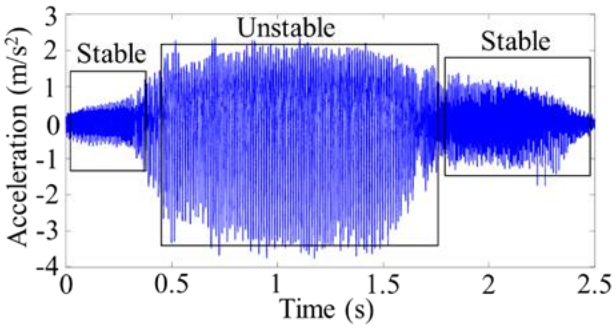

Figure 6. Raw data acquired in the turn-milling process

(a) (b) (c)

Figure 7. The potential differences in the chip morphology obtained in; (a) turning, (b) milling, and (c) turn-milling

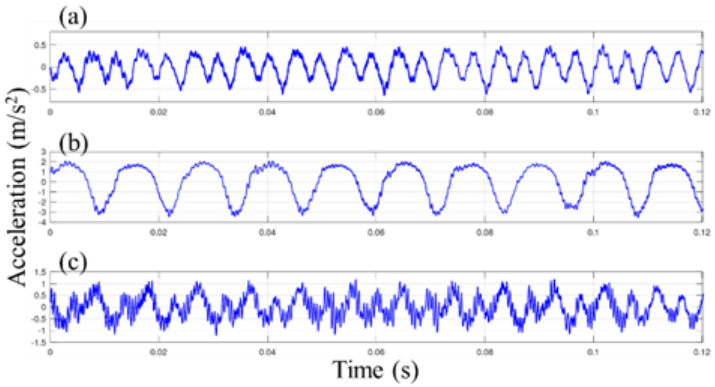

Figure 8. Sampled signal of full signal; (a) stable signal in the left region, (b) unstable signal in the middle region, and (c) stable signal in the right region

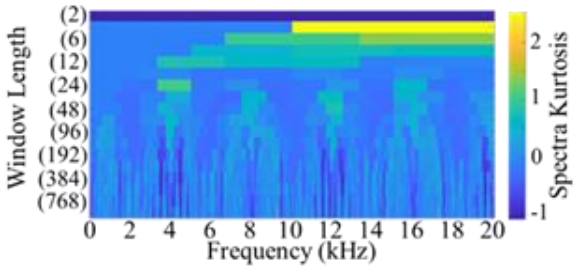

(a)

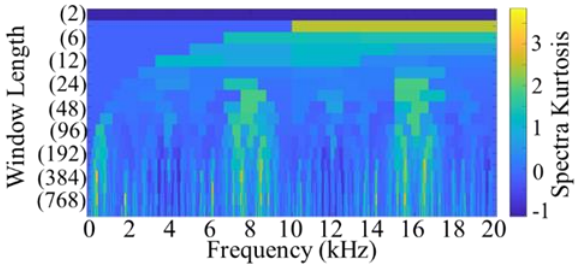

(b)

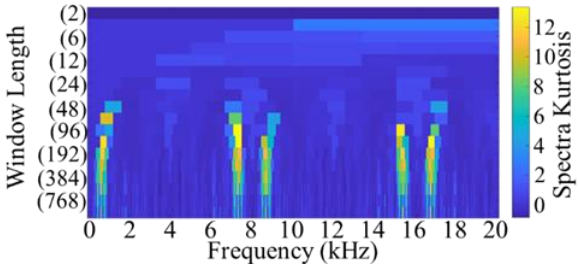

(c)

Figure 9. Spectral kurtosis which corresponding to the sampled signal; (a) spectral kurtosis of stable signal in the left region, (b) spectral kurtosis of unstable signal in the middle region, and (c) spectral kurtosis of stable signal in the right region

That full signal is explored by sampling it becoming a portion of some signals as shown in Figure 8. This sampling data consist of 50.000 data. This figure represents the vibration signal for each condition; Figure 8(a) is the sampling signal for stable machining in the left region, Figure 8(b) is the sampling signal for unstable machining in the middle region, and Figure 8(c) is the sampling signal for stable machining in the right region. Now it can be seen that vibration signals are showing distorted oscillation waves rather than

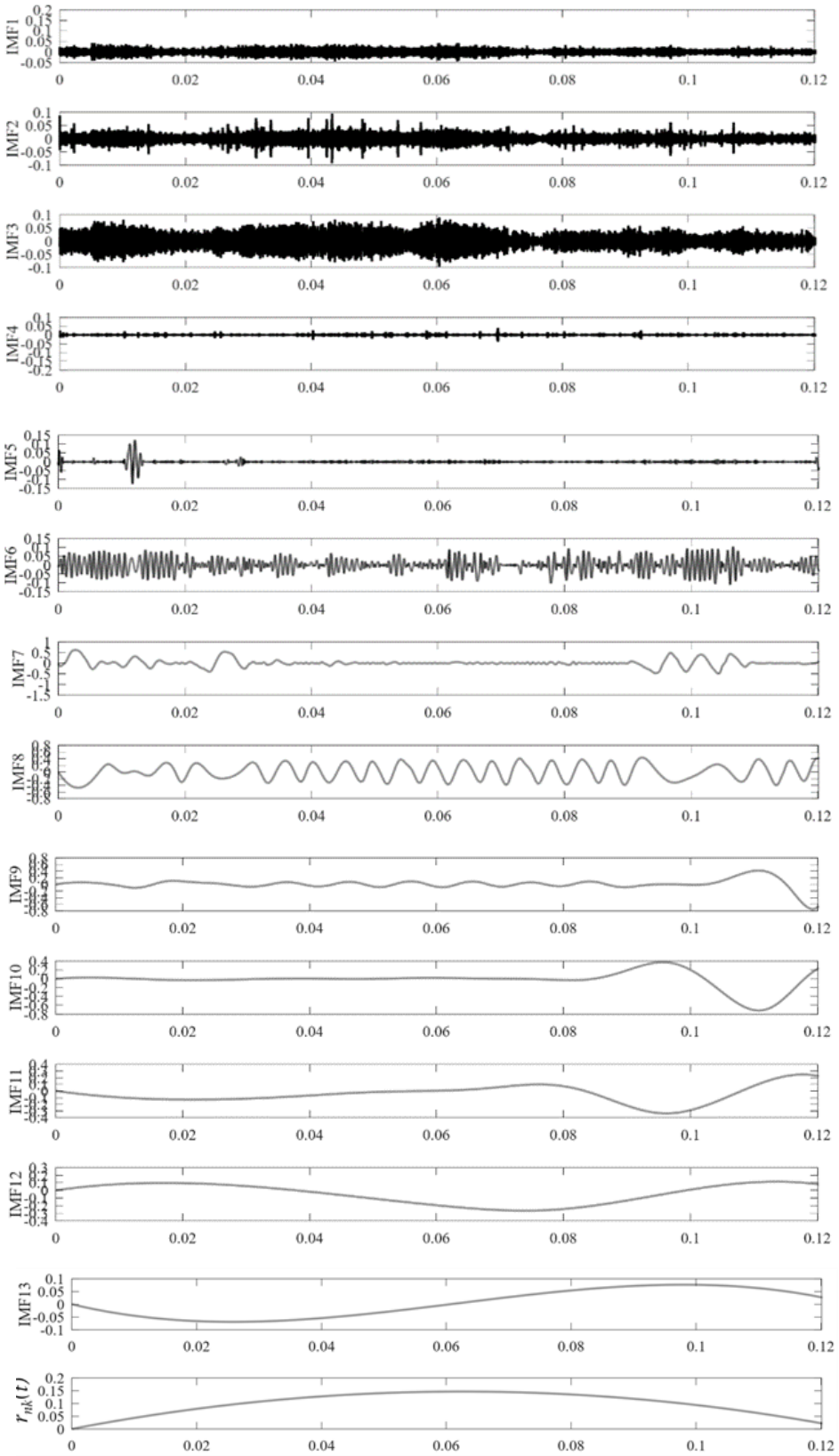

Figure 10. IMF components corresponding to the stable signal in the left region

showing clear sinusoidal signals. Next step, kurtosis index, and spectral kurtosis were employed to prove that deduction. Figure 9 shows the results of kurtosis index, and spectral kurtosis.

Figure 9(a) is spectral kurtosis which corresponds to the sampled signal in the left region. This spectral indicates that the frequency band is centered at 1.5 kHz in level 4

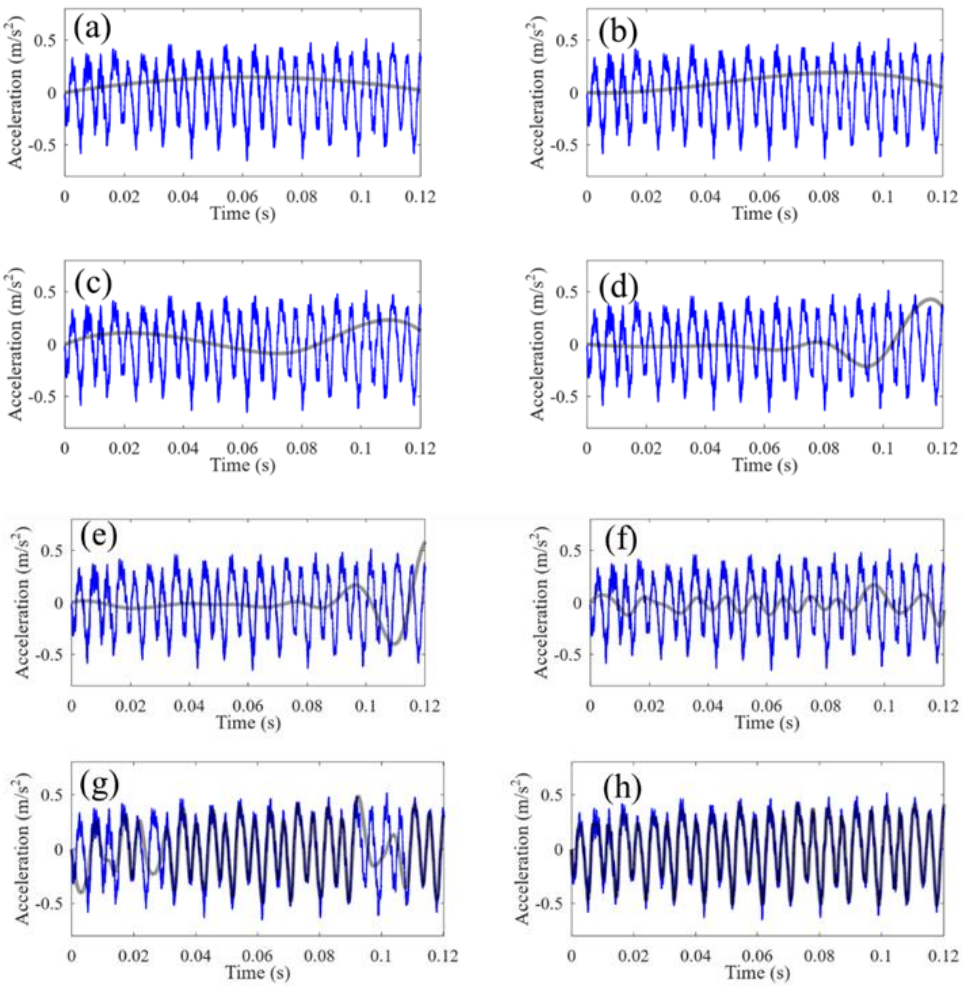

Figure 11. The process of filtering data through reconstruction of the IMFs

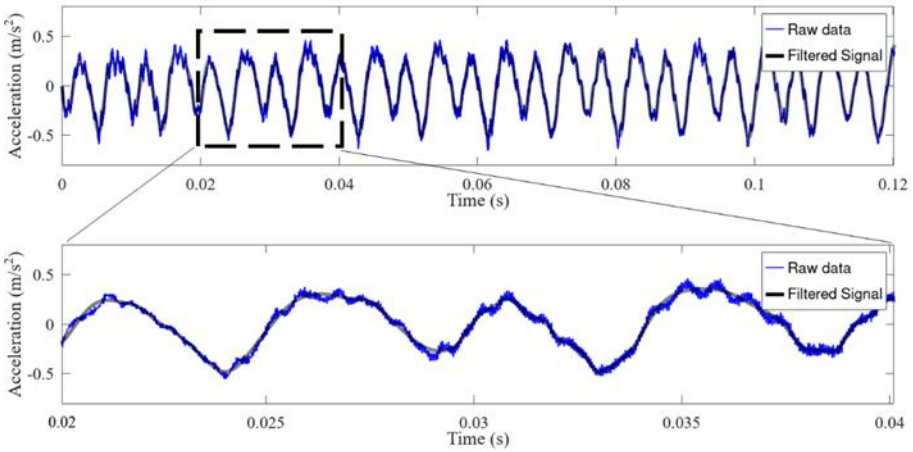

Figure 12. Comparison between raw signal and filtered signal from noise resulted from reconstructing IMFs

with a bandwidth of 10 kHz and contains the highest kurtosis of 2.54. Figure 9(b) shows spectral kurtosis which corresponds to the sampled signal in the middle region. In this spectral, the frequency band is centered at 1.8 kHz in level 8.6 with a bandwidth of 0.5 kHz and contains the highest kurtosis of 3.9. Figure 9(c) shows spectral kurtosis which corresponds to the sampled signal in the right region. In this spectral, the frequency band is centered at 7.3 kHz in level 96 with a bandwidth of 0.4 kHz and contains the highest kurtosis of 13.4.

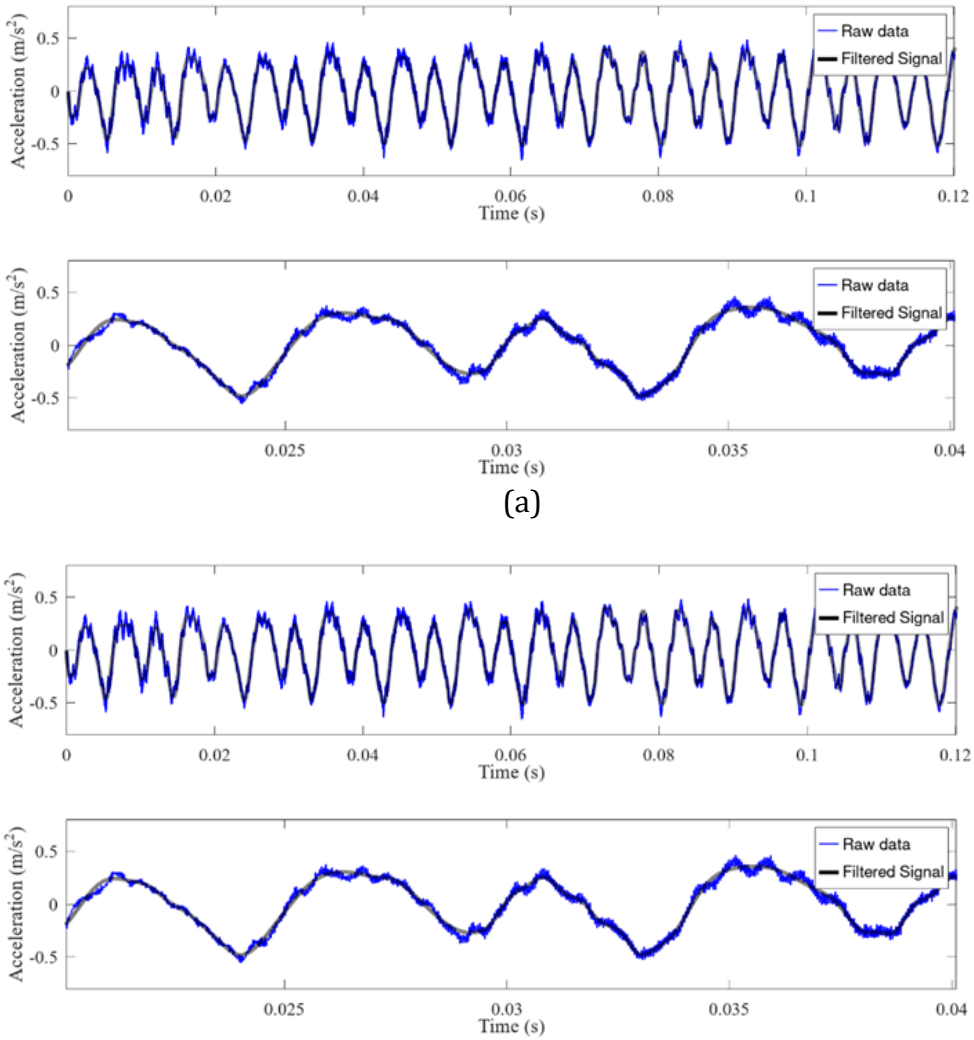

Figure 13. Comparison between raw signal and filtered signal resulted from reconstructing IMFs; (a) Reconstructed signal corresponding to signal in Figure 8(b), (b) Reconstructed signal corresponding to signal in Figure 8(c)

From the figures, spectral kurtosis provides a blocked and blurry spectrum. It can be seen that the spectral kurtosis method fails to detect the resonant frequency band to inform the current turn-milling condition. Besides, the noises which are contaminated the vibration signal made any problem revealing the machining. Next, those vibration signals are going to be denoised using EMD for enhancing the signal-to-noise ratio. Therefore, it is a key pre-processing step before further analysis.

All vibration signals in Figure 8 are decomposed by EMD to be a set of IMFs and a residual process. Figure 10 shows IMFs corresponding to vibration in the top panel of Figure 8 (stable machining in the left region). 13 IMFs and a monotonic residue were obtained by this process. It is seen that EMD arranges the IMFs from the IMF with the most oscillations to IMF with the least oscillations. It means that c_1 contains the highest frequency and c_{13} contains the lowest frequency with different oscillation amplitudes. The monotonic residue is the signal containing no more an oscillation, but it will be included in the consideration of the reconstruction signal technique later.

Reconstruction of those IMFs will give a filtered signal from the noise. This technique is performed by adding the IMFs and the process is shown in Figure 11. In this figure, the black signal is the step of the reconstruction technique in detail and they are compared to the raw signal (blue signal).

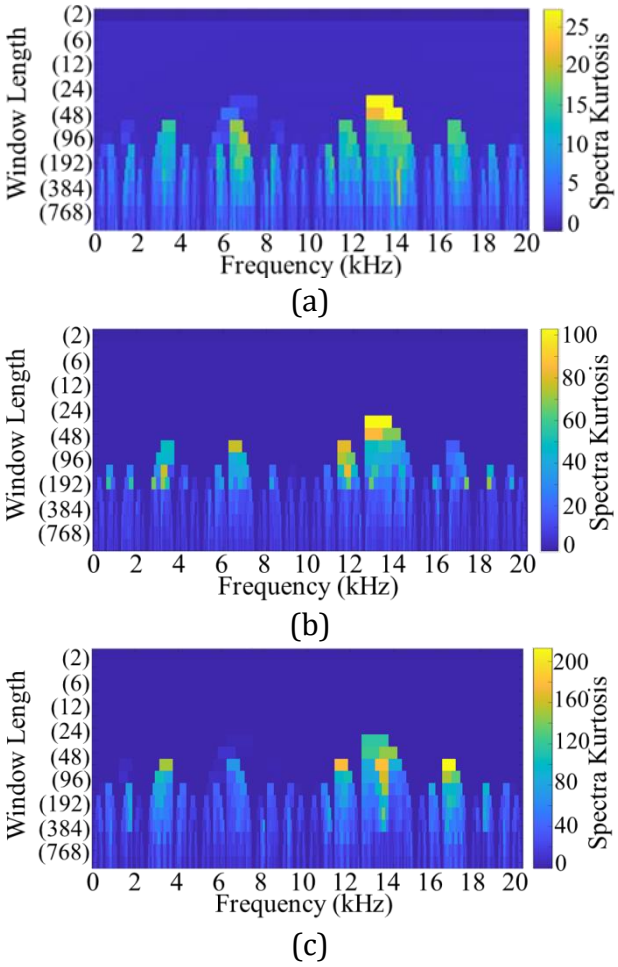

Figure 14. Spectral kurtosis which corresponding to the filtered signals; (a) spectral kurtosis of filtered signal in Figure 12, (b) spectral kurtosis of filtered signal in Figure 13(a), and, (c) spectral kurtosis of filtered signal in Figure 13(b)

Figure 11(a) shows the comparison between the monotonic residue, $r_{nk}(t)$ to the raw data. By itself, the fitting of the monotonic residue is not comparable to the raw signal. Let us add the monotonic residue to the IMF13 component, $r_{nk}(t) + c_{13}(t)$, and it is shown in Figure 11(b). Now, it shows one oscillation completely, but it is still not comparable to the raw signal and the aim of the research is not achieved yet. By serially adding more IMF components with increasing frequency, the results are shown in the series of Figure 11. Figure 11(c) is adding of $r_{nk}(t) + c_{13}(t) + c_{12}(t)$, Figure 11(d) is $r_{nk}(t) + c_{13}(t) + c_{12}(t) + c_{11}(t)$, Figure 11(e) is $r_{nk}(t) + c_{13}(t) + c_{12}(t) + c_{11}(t) + c_{10}(t)$, Figure 11(f) is $r_{nk}(t) + c_{13}(t) + c_{12}(t) + c_{11}(t) + c_{10}(t) + c_9(t)$, Figure 11(g) is adding of $r_{nk}(t) + c_{13}(t) + c_{12}(t) + c_{11}(t) + c_{10}(t) + c_9(t) + c_8(t)$. It successively improves and gets more fitting to the raw data. The last construction technique is shown in Figure 11(h) by adding of $r_{nk}(t) + c_{13}(t) + c_{12}(t) + c_{11}(t) + c_{10}(t) + c_9(t) + c_8(t) + c_7(t)$. Those last seven IMF and monotonic give the filtered signal from noise. This comparison of two signals is zoomed out the picture as shown in Figure 12. As can be seen, the new signal is now quite impressive compared to the raw signal and the oscillation of the filtered signal is clearer than the raw signal.

From above result, reconstruct the monotonic residue to the filtered signal gives the gradual change. The components with the highest frequencies add a little more energy, but they make the data look more complicated.

In the next step, the EMD had been applied for decomposing the signals in Figures 8(b) and 8(c) as well. In those decompositions, 13 IMFs and a monotonic residue were also obtained for each signal. The step is similar to the previous vibration data and

therefore it directly shows the comparison between the raw signal and the filtered signal obtained from reconstructing IMFs as shown in Figures 13(b) and 13(c). It is seen that the new signal is now quite impressive compared to the raw signal and the oscillation of the filtered signal is clearer than the raw signal.

To see the improvement of the filtered signals, the kurtosis index and spectral kurtosis were applied again to filtered signals and the spectral is shown in Figure 14. As can be seen from the figures, the spectra display different features compared to spectral kurtosis in Figure 9 and the kurtosis index is improved greatly. Figure 14(a) contains the highest kurtosis of 27.2, and Figure 14(b) contains the highest kurtosis of 102. Figure 14(c) contains the highest kurtosis of 212. The kurtosis index had been improved 10 – 27 times more than the raw signal. It means that the filtered signals have enhanced their signal-to-noise ratio.

Analysis Signal Using STFT

In order to find out important information on the view of machining process monitoring, those signals are further analysed in time-domain frequency short-time Fourier transform (STFT) to get STFT spectra. The spectra were used to examine the phenomena that happened during machining based on their energy and frequency content.

This signal processing tool was applied to all raw vibration signals and reconstructed vibration signals. The resulted STFT spectrums corresponding to the raw vibration signal are shown in Figure 15. Figure 15(a) is the STFT spectrum of raw vibration signal corresponding to stable signal in the left region (see Figure 7(a)), and Figure 15(b) is the STFT spectrum of raw vibration signal corresponding to unstable signal in the middle region (see Figure 8(b)), and Figure 15(c) is STFT spectrum of raw vibration signal correspond to unstable signal in right region (see Figure 8(c)).

It is seen from Figure 15(a) that the energy in the STFT spectrum focuses on the spindle frequency, namely 50 Hz for spindle rotational frequency $\left(f_{sp} = {}^{\omega}/_{60}\right)$. It means that the mechanical structure had been excited by forcing force at the low frequency of machining. In the view of mechanical vibration, this kind of vibration is not harmful. It has to be taken to highlight that STFT provides a blurry energy spectrum in this case. Based on the spectrum in Figure 15(b), some frequencies appear marked by appearing some energy in the STFT spectrum. With a bit difficulty in spectrum identification because of the blurry spectrum, those frequencies are spindle rotational frequency (50 Hz), 200 Hz for the frequency of tooth passing $\left(f_p = N_t \cdot f_{sp}\right)$, its harmonic frequencies whose was calculated by multiply integer number to f_p, and natural frequency of the cutting system (f_n = 1 kHz). These kinds of frequencies are well-known as the characteristic frequencies of the machining process. Because many frequencies appear in the spectrum, working under this forced vibration is then certainly harmful. Besides, the spectrum in Figure 15(c) provides the energy in the STFT spectrum focusing on the spindle frequency again with the energy highest than the spectrum provided in Figure 15(a). It was related that the machining process is in stable condition.

Those spectra provide a blurry spectrum; therefore, it was difficult to find information related to the machining process condition. It might be caused by some noises that was backgrounded in the main vibration data. Let us now apply the STFT to reconstructed data to get a new insight into the spectrum as shown in Figure 16. Figure 16(a) is the STFT spectrum of the reconstructed signal corresponding to the signal in Figure 12, Figure 16(b) is the STFT spectrum of the reconstructed signal corresponding to the signal in Figure 13(a), and Figure 16(c) is STFT spectrum of reconstructed signal correspond to signal in Figure 13(b). It is looks that the spectra are better than the

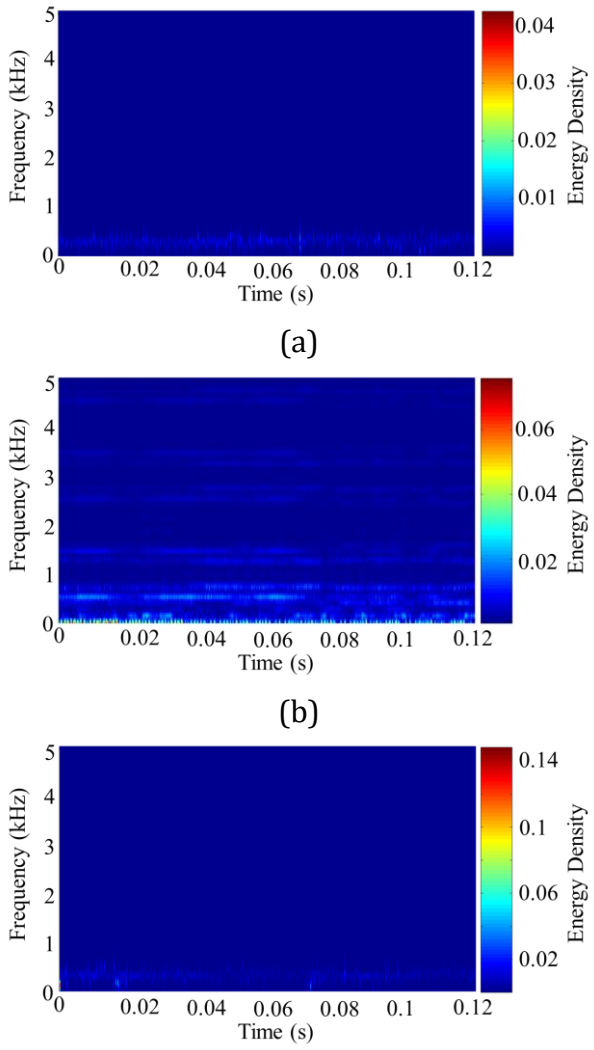

Fig 15. STFT spectrum of raw vibration signal; (a) STFT spectrum of raw vibration signal corresponds to vibration in Figure 7(a), (b) STFT spectrum of raw vibration signal corresponds to vibration in Figure 7(b), (c) STFT spectrum of raw vibration signal corresponds to vibration in Figure 7(c)

previous spectra. Let us pay attention to the spectrum in Figure 15(b). Here, this spectrum shows a messy energy at many frequencies and makes it easy to identify that the chatter vibration potentially aroused in the turn-milling process. On the other hand, the density energy for each spectrum also changes drastically compared to the STFT spectrum without improvement using EMD. The density energy had been increased 10 – 100 times larger.

The above results show that the STFT-based method shows its capability for turn-milling process monitoring and generally many people have used it. However, some limitations of STFT also had been found, namely, STFT provided a blurry spectrum when some noises contaminated the main vibration data. It is therefore EMD that was used to filter the raw vibration efficiently and adaptively to get new clear data by the reconstruction technique of IMFs. The reconstructed signals were then evaluated in the time-frequency domain using STFT, which represents the time–frequency–energy distribution of analyzed signals. Above results show the utilization of the empirical mode decomposition (EMD) method as an efficient and adaptive noise filter. The Short-Time Fourier Transform (STFT) shows significant performs in its spectrum when EMD was

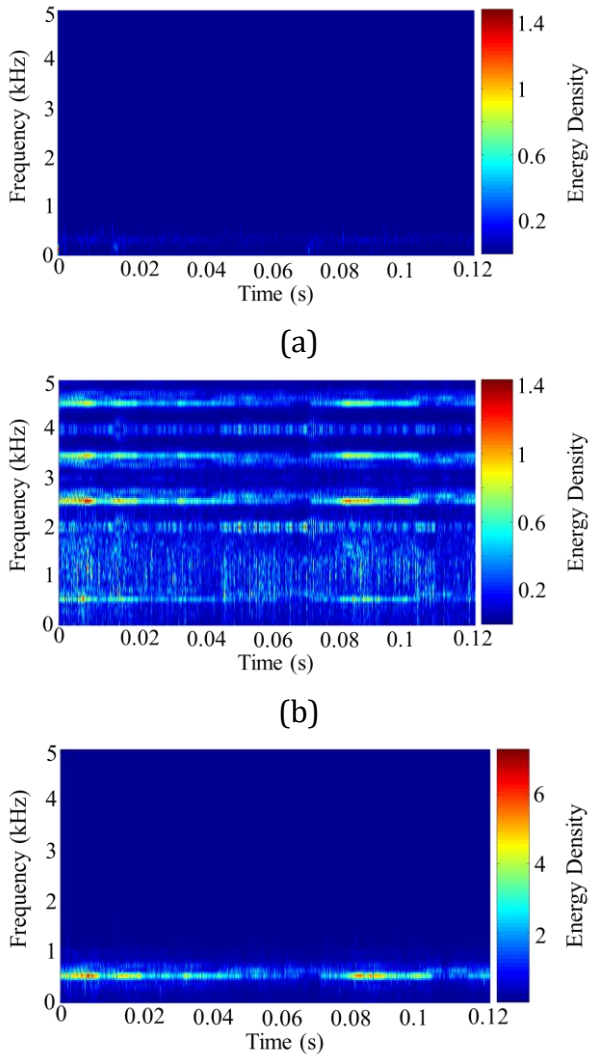

Fig 16. STFT spectrum of raw vibration signal; (a) STFT spectrum of the reconstructed signal corresponds to vibration in Figure 10, (b) STFT spectrum of the reconstructed signal corresponds to vibration in Figure 11(a), (c) STFT spectrum of the reconstructed signal corresponds to vibration in Figure 11(b)

applied. On the other word, the improved STFT using EMD showed a significant spectrum with high resolution compared to conventional STFT. The combination of EMD-STFT made it easy to identify the machining condition and the proposed method was effectively applied to monitor the turn-milling condition.

CONCLUSIONS

Measured vibrations are generally backgrounded by noise. It is, therefore, necessary to find efficient and adaptive signal processing tools for denoising noisy signals before further analysis. This article presented a working combination of EMD-STFT for monitoring the turn-milling condition. Empirical mode decomposition (EMD) was used as a filter of noisy raw vibration data by reconstruction IMFs. The clear data was further analysed by STFT in the time-frequency domain. The results show that the reconstructed signal was quite impressive compared to the raw signal and the oscillation of the filtered signal was clearer than the raw signal. The improvement of the filtered signals was proved

by the kurtosis index and spectral kurtosis. The kurtosis index had been improved 10 – 27 times more than the raw signal.

The STFT-based method shows its capability for turn-milling process monitoring. However, some limitations of STFT also had been found, namely, STFT provided a blurry spectrum when some noises contaminated the main vibration data. After the raw data was denoised using EMD, the STFT displays a clear spectrum and made it easy to identify the machining condition. The energy density proved that. EMD worked efficiently and adaptively to filter the raw vibration from background noise.

ACKNOWLEDGEMENTS

The authors would like to be obliged to the Centre for Industrial Research, National Research and Innovation Agency of Indonesia (BRIN) for providing the research equipment and Ministry of Research and Education of Indonesia who has provide funding for this research on DIPA No. SP-DIPA 023.18.1.690524/2022.

DECLARATION OF CONFLICTING INTERESTS

The author(s) declared no potential conflicts of interest with respect to the research, authorship, and/or publication of this article.

FUNDING

The author(s) disclosed receipt of the following no financial support for the research, authorship, and/or publication of this article. The authors would like to be obliged to the Ministry of Research and Education of Indonesia who has provide funding for this research on DIPA No. SP-DIPA 023.18.1.690524/2022.

REFERENCES

[1] Karaguzel, U., Bakkal, M., and Budak, E. Process modeling of turn-milling using analytical approach, in Procedia CIRP, Vol. 4, p. 131–139, 2012.
[2] Kara, M. E. and Budak, E. Optimization of Turn-milling Processes, Procedia CIRP, Vol. 33, p. 476–483, 2015.
[3] Ratnam, C., Vikram, K.A., Ben, B.S., end et al., Process monitoring and effects of process parameters on responses in turn-milling operations based on SN ratio and ANOVA. Measurement, Vol. 94, p. 221-232, 2016.
[4] Choudhury SK., and Mangrulkar K.S. Investigation of Orthogonal Turn-milling for the Machining of Rotationally Symmetrical Workpieces. J. Mater Process Technology, Vol. 99, p. 120–128, 2000.
[5] Choudhury SK., Bajpai J.B., Investigation in Orthogonal Turn-milling Towards Better Surface Finish. Journal of Material Processing and Technology, Vol. 170, 487-493, 2004.
[6] Kopac J., and Pogacnik M. Theory and Practice of Achieving Quality Surface in Turn Milling. Int. Journal of Machine Tools Manufacture. Vol. 37, No. 5, 709-715, 1995.
[7] Yuan S., and Zheng W., The Surface Roughness Modelling on Turn-milling Process and Analysis of Influencing Factors. Applied Mechanics and Materials, Vol. 117-119. p. 1614-1620, 2012.
[8] Huang C., and Cai Y, Turn-milling Parameters Optimization Based on Cutter Wear. Advanced Materials Research Vol. 602-604. p. 1998-2001, 2013.
[9] Karaguzel U., Olgun U., Uysal E., end et al., High Performance Turning of High Temperature Alloys on Multi-tasking Machine Tools: New Production Technologies in Aerospace Industry, Lecture Notes in Production Engineering; p. 1-9, 2014.

[10] Neagu C., Gheorghe M., and Dumitrescu A. Fundamentals on Face Milling Processing of Straight Shafts. J Material Processing and Technology, Vol.166, 337–344, 2005.
[11] Filho J. Prediction of Cutting Forces in Mill-Turning Through Process Simulation using a Five-axis Machining Centre. The International Journal of Advanced Manufacturing Technology, Vol. 58, 2012.
[12] Tamang, S., and Chandrasekaran, M. Multi-objective Optimization of Turning Performance Characteristics using GA Coupled with AHP based Approach. International Journal of Integrated Engineering, 13(6), 126–136, 2021.
[13] Rachmat, H., and Rafai, N. H. The Effect of Drill Reamer Tool on Cutting Force and Temperature when Machining with Different Parameters and Cutting Condition. International Journal of Integrated Engineering, 12(2), 206–210, 2020.
[14] Susanto, A., Yamada, K., Tanaka, R., end et al., Chatter identification in turning process based on vibration analysis using Hilbert-Huang transform", J. Mechanical Engineering and Science, Vol. 14, No. 2, p. 6856–6868, 2020.
[15] Susanto, A., Liu, C.H., Yamada, K., end et al., Milling Process Monitoring Based on Vibration Analysis Using Hilbert-Huang Transform, Int. J. Automation Technology, vol. 12, no. 5, p. 688–698, 2018.
[16] Ismail, M. F., Jamian, R., Yahaya, M. I., end et al., Surface Metrology for Process Diagnostic of Ultrasonic Vibration Assisted Grinding. International Journal of Integrated Engineering, 14(5), 215–222, 2022.
[17] Gupta, P., Singh, B., and Shrivastava. Y., Robust Techniques for Signal Processing: A Comparative Study. Evergreen; Joint Journal of Novel Carbon Resource Sciences & Green Asia Strategy, Vol. 09, Issue 02, 404-411, 2022.
[18] Susanto, A., Liu, C. H., Yamada, K., end et al., Application of Hilbert–Huang transform for vibration signal analysis in end-milling, Precis. Eng., vol. 53, no. April, pp. 263–277, 2018.
[19] Z. Zhang, H. Li, X. Liu, end et al., Chatter mitigation for the milling of thin-walled workpiece, Int. J. Mech. Sci., vol. 138–139, pp. 262–271, 2018.
[20] Harun, M. H. S., Ghazali, M. F., and Yusoff, A. R., Tri-axial Time-frequency Analysis for Tool Failures Detection in Deep Twist Drilling Process, Procedia CIRP, vol. 46, pp. 508–511, 2016, doi: 10.1016/j.procir.2016.03.128.
[21] Huang, N.E., and Shen, S.S.P. Hilbert–Huang Transform and Its Applications, vol. 2. World Scientific Publishing, 2005.
[22] Susanto, A., Yamada, K., Mani, K., end et al., Vibration Analysis in Milling of Thin-Walled Workpieces Using Hilbert-Huang Transform, in 9th International Conference on Leading Edge Manufacturing in 21st century: LEM21, vol. 9, pp. 1–6, 2017.
[23] Susanto, A., Yamada, K., Tanaka, R., end et al., Analysis of Transient Signal using Hilbert-Huang Transform for Chatter Monitoring in Turning Process. The 4th International Conference on Information Technology, Information Systems and Electrical Engineering, p. 26–30, 2019.
[24] Cao, H., Lei, Y., and He, Z. Chatter identification in end milling process using wavelet packets and Hilbert-Huang transform. Int. J. Mach. Tools Manuf., vol. 69, p. 11–19, 2013.
[25] Huang, N.E., Wu, Z., Parkinson, C.L., end et al., Reductions of Noise and Uncertainty in Annual Global Surface Temperature Anomaly Data. Adv. Adapt. Data Anal., vol. 1, no. 3, p. 447–460, 2009.